Simulation of a typical reentry vehicle TPS local flow features and material response

E. V. Titov, and D. A. Levin

Pennsylvania State University, University Park, PA 16802

Abstract. Statistical BGK/DSMC and continuum N-S simulations of a typical vehicle reentry flow were performed taking into account local flow features. The local surface features were known to cause problems during the Apollo era Earth atmosphere reentry Ref. [1] and therefore require close attention as the shapes and design details of the new reentry vehicles tend to build on the Apollo reentry capsules. The TPS thermal response to the high energy reentry flow in cracks and compression pad areas is important to understand to predict the TPS degradation due to the chemical and thermal ablation. The TPS study presented in this article includes the stagnation area micro crack and compression pads which disturb the flow and cause local augmentation of heat flux, which in turn, results in higher recession rates.

THE UNDERLYING PHYSICS

The AVCOAT TPS, studied here, is under a thermal (convective and radiative) as well as a mechanical load due to the shear stress. There are three distinct portions of the charring TPS material. The intact layer consists of the virgin epoxy novalac resin and silica-fiber substrate bounded by the fiber-glass honeycomb matrix. The pyrolysis zone on top of the virgin material is an active layer, where, because of the conducted heat, the chemical reactions releasing the pyrolysis gases occur. The pyrolysis gases, whose elemental composition is presented in Table 1 (reproduced from Ref. [2]), escape from the pyrolysis zone through the porous residual char layer and enter the boundary layer, helping to release heat and also partly blocking the char surface chemical reactions causing the recession. The char layer above the pyrolysis zone consists mostly of carbon and silica. The char layer is still bounded by the honeycomb matrix but both the char and the matrix materials are recessing. The elemental composition of the char is presented in Table 1 as well. The major char surface reactions are presented in Table 2 and are the contributors to the char surface recession. Another contributor to the recession is a mechanical erosion of the char due to the boundary layer shear [3], but it is not considered here. Two cases are considered in this article. The first case is a rarefied flow arcjet case aimed at studying of the stagnation area micro-crack in anticipation of the NASA tests of the new TPS systems. The second case, a 95 km CEV flow with local features, is an application of the technique to a practical problem concerned with flow disturbance at the compression pad areas in the rarefied flow at an altitude of 95 km.

THE MODELING PROCEDURE

For the dense flow arcjet cases we chose the statistical BGK, coupled with the DSMC solver, as a technique capable of handling the challenges posed by this research problem instead of a pure CFD or DSMC approach because they have limited range of applicability or prohibitive computational cost. The variation of the Knudsen number computed based on the crack inlet diameter along the crack wall is presented in (A) portion of Fig 1. As can be seen in the figure the variation is small for this stagnation area crack flow and the characteristic Knudsen number is 0.001. At these levels of Knudsen number the baseline DSMC technique becomes prohibitively expansive. On the other hand traditional CFD tools lack accuracy of modeling the complex boundary conditions such as thermal and chemical ablation in this flow regime that can be characterized as slip. The BGK technique applied in this research is computationally effective at these Knudsen numbers and also allows effective ablation modeling at the particle level.

The computational domain for the stagnation point crack cases includes a portion of the flow in front of the crack. The crack inlet boundary conditions were set at all of the boundaries of the computational domain except for the walls and are given in Table 3. The inlet boundary conditions for the micro-crack problem were obtained from a N-S/CFD [4]

solution. The inlet boundary was located behind the shock for all of the BGK cases with the shock layer solved with the N-S technique.

The boundary conditions at the wall of the crack and at the surface of the TPS facing the flow were the full energy and momentum accommodation, at a temperature of 1831 K. In addition, the reactions presented in Table 2 were allowed to occur at the crack walls. The pyrolysis gases, emerging from the surface, whose elemental composition is presented in Table 1 were assumed to be in the molecular (not elemental) state and were assumed not to contribute to the flow-surface chemistry. Such an assumption is consistent with findings provided in Ref. [5] and is based on the following concepts. The pyrolysis gases are in chemical equilibrium at the wall temperature and pressure in the boundary layer region. At the temperatures below 3000K, the pyrolysis generated C and O can form CO and molecular oxygen. However, since the proportion of elemental carbon atoms to atomic oxygen is such that the latter is the limiting reactant, all available atomic oxygen is consumed by the reaction with atomic carbon to form CO with no atomic oxygen remaining to produce the molecular oxygen. The excess of atomic carbon is expected to form either CN, or C_2 or remain in the elemental state, but since the excess of atomic carbon was small these reactions were not taken into account. For the same reason the elemental carbon, hydrogen, nitrogen and silicon were not modeled as parts of the pyrolysis gases. The recession of the wall occurs as the residual char layer is being oxidized and nitridised by the flow radicals. The recession rate is computed assuming a local flow equilibrium approach similar to the technique presented in [6].

RESULTS AND DISCUSSION

The statistical BGK modeling of the specimen crack area, performed in this study, required the flow quantities behind the shock wave to setup the inlet boundary conditions. These quantities were obtained from a computational fluid dynamics (CFD) analysis. A fully viscous Navier-Stokes solution of the JSC conical nozzle arc-jet was generated with the Data-Parallel Line Relaxation (DPLR) solver where the arc-jet nozzle and the stagnation-point calorimeter were simulated simultaneously at the chosen test condition. The DPLR software package is a suite of CFD tools for the computation of supersonic and hypersonic flows in chemical and thermal non-equilibrium [4].The simulation took advantage of the axial symmetry of both the nozzle and the calorimeter geometry. The finite-rate reaction kinetics was modeled with Park's 5-species air chemistry. The obtained parameters are presented in the first column of Table 3.

Two stagnation point crack cases assuming axial symmetry of the flow were modeled using the BGK technique with one of them solved for times 0 and 20 seconds of exposure time in the arcjet. These cases were: (a) with chemical ablation only and (b) with both thermal and chemical ablation. Numerical parameters of the scheme are presented in Table 4. A comparison of the basic flow parameters for cases (a) and (b) is presented in Fig. 1. Several observations can be drawn from the figure. The first observation is that the pressure level inside the crack is higher than the flow stagnation pressure (which for this case is 1.881×10^5 Pa.) This observation can be made for both cases and for the case with both chemical and thermal ablation the pressure increase is larger than for the case with only chemical ablation (Fig. 1(A)). The predicted pressure rise above the flow stagnation pressure is a valid result (although it may be not intuitive). In the case of chemical ablation the lighter atoms of oxygen and nitrogen are replaced with heavier products of the flow-surface reactions, namely CO and CN. This mass increase causes the pressure rise as the heavier molecules exert more pressure because they carry more kinetic energy. In the case with both types of ablation the effect is even larger as a result of the insertion of the heavier pyrolysis gas molecules (CO) into the flow.

A second observation can be made regarding the flow behavior inside the crack in Fig. 1(B and D) where the flow velocity and streamlines are presented. The flow velocity is predictably small inside the crack, however there is a qualitative difference between the flow pattern for two ablation cases, observed in Fig. 1(D). In the case of chemical ablation the flow forms re-circulation areas and is probably unstable (although only the steady state solutions were obtained in this study). The developed vortices may play a significant role in the removal of the ablation components from the cavity, thereby influencing the crack wall recession rate. In the case of chemical and thermal ablation such vortices are not observed with a slow flow of the pyrolysis gases outward the crack being developed instead.

Figure 1 also presents the flow species composition inside the crack and in front of it. Portions (E) and (G) of Fig. 1 present chemically active species (atomic oxygen and nitrogen) mole fractions and portions (F) and (H) present the product mole fractions of the chemical ablation and pyrolysis. It can be observed in portions (F) and (H) of Fig. 1 that in case of chemical ablation the major species residing inside the crack are products of the ablation: CN and CO. Both of their mole fractions are significant inside the crack but rapidly decrease outside the crack. In the case of both types of ablation the dominant species inside the crack is CO, which is due to its presence in both the products of the chemical ablation and the pyrolysis gases emerging from the crack surface.

It can also be observed in portions (E) and (G) of Fig. 1 that despite the significant differences in the chemical composition and the structure of the flow in the crack, the amount of chemically active atomic oxygen and nitrogen is relatively small at the crack channel walls. This results in small surface recession rates inside the crack with the tendency of the recession rate to have a significant increase closer to the entrance of the crack where the free-stream atomic oxygen and nitrogen are still able to penetrate the crack boundary layer and react with the crack surface.

In order to understand the degree of the surface recession, the rate computed for the case with both types of ablation was used to morph the crack surface. The morphing procedure, described in details in Ref. [7] with additional explanations given in Ref. [8], was based on the local recession rate at each of the locations along the crack wall. In the case of two dimensional flows the procedure is simple as it works on the linear fragments of the specimen body representation as opposed to 3D surfaces in the three dimensional cases. The underlying principle of the procedure is to use the local oxidation rates to move the nodes of the surface meshes accordingly. The procedure assumes that the oxidation rates are constant for a period of time (20 sec in this research), but recomputes the normal directions at each of the surface mesh nodes after smaller (1 sec) increments to keep the direction of the node movements in a more realistic way. The procedure was performed assuming the flow impact duration of 20 seconds with the resulting crack shape presented in Fig. 2.

Figure 2 presents the BGK solution of a case with an advanced (20 seconds) crack shape. This case involved both types of ablation in order to take into account all the protective mechanisms available for AVCOAT. Figure 2 presents the flow species composition inside the crack and in front of it. It can be seen in the figures that the flow pattern inside the cavity is similar to that of the original (not recessed) case involving both types of ablation, however, key differences can also be observed in the vicinity of the crack inlet. These differences include larger amounts of atomic oxygen and nitrogen mole fractions at the wall close to the crack inlet (see portions A and C of Fig. 2). This will translate into higher recession rates in this region resulting in a greater impact on the TPS integrity. One more interesting observation can be made in portion (D) of Fig. 2 where a sudden increase in the CN mass fraction is present at the edge of the crack inlet. The CN radical is not a one of the pyrolysis gases modeled in this case since the CO is the pyrolysis dominant species. This spike in the CN mole fraction occurs due to a greater boundary layer penetration by the atomic nitrogen causing an increase in the chemical ablation at the crack inlet area. The preliminary conclusion from this observation is that the thermal ablation is the primary protection mechanism for the cavities with chemical ablation taking over in places where the thermal ablation protection fails.

An additional case solved here was a compression pad flow. The flow configuration features a cavity on the shoulder of the CEV TPS. The case involved free stream conditions corresponding to an altitude of 95km along the CEV projected trajectory as presented in Table 3.The case flow regime makes it to be solvable by the baseline DSMC method which was applied. The TPS surface was assumed to be AVCOAT and the modeling procedure was the same as in the Acjet cases except that the pyrolysis gases were assumed to be emerging from the entire TPS syrface except for the compression pad area. The wall oxidation and nitridation boundary conditions were applied at the entire TPS surface including the compression pad areas. The results are presented in Fig. 3. The LHS of the figure presents the flow density while the RHS presents the flow stream traces and velocity vectors in vicinity of the compression pad. The flow pattern in the vicinity of the compression pad cavity can be characterized as closed according to Ref. [9]. This provides a basis for a conclusion regarding the applicability of the local heating augmentation model provided in Ref. [9]. Based on the model presented in Ref. [9] and the previous works of the authors of this abstract [10, 6] a prediction about a nonuniform recession rates resulting in the nonuniform vehicle TPS surface degradation can be made with implications to the vehicle safety during the atmosphere entry.

ACKNOWLEDGMENTS

REFERENCES

1. R. Thompson, V. Lessard, T. Jentik, and E. V. Zoby, *AIAA Paper 2009-1575* (2009).
2. E. P. Bartlett, L. W. Anderson, and D. M. Curry, *Journal of spacecrafts and rockets* **8** (1971).
3. R. A. Graves, and W. G. Witte, *NASA Technical Note TN D-4713* (1968).

4. M. J. Wright, G. V. Candler, and D. Bose, *AIAA Journal* **36**, 1603–1609 (1998).
5. J. E. Pavlovsky, and L. G. Leger, *NASA Technical Note D-7564* (1974).
6. E. Titov, J. Zhong, D. Levin, and D. Picetti, *Journal of Thermophysics and Heat transfer* (2009).
7. E. Titov, J. Zhong, D. Levin, and D. Picetti, *18th AIAA Computational Fluid Dynamics Conference, AIAA Paper No. 2007-4469* (2007).
8. E. Titov, J. Zhong, D. A. Levin, and D. J. Picetti, *Thermophysics and Heat Transfer* (Submitted for puplication in 2009).
9. B. Hollis, *AIAA 2009-3843* (2009).
10. E. Titov, D. Levin, D. Picetti, and B. Anderson, *AIAA Paper No. 2009-3599,41st AIAA Thermophysics Conference, 22-25 June 2009* (????).
11. D. Olynick, Y. Chen, and M. E. Tauber, *Journal of spacecrafts and rockets* **36** (1999).

TABLE 1. Elemental composition of the pyrolysis gases and the residual char [2].

Element	Pyrolysis gas	Char
H	0.1311	-
C	0.3614	0.614
N	0.0268	-
O	0.4807	0.206
Si	-	0.180

TABLE 2. List of thermal ablation ablation reactions for AVCOAT. [11]

| No.	Reaction	probability [2]
1	$C_{surface} + O_{flow} \rightarrow CO$	0.9
2	$C_{surface} + N_{flow} \rightarrow CN$	1.0

TABLE 3. Inlet conditions for the Arcjet (from the presented DPLR arcjet solution) case and the CEV 81 km. case (MSIS-E-90 Atmosphere model)

	Arcjet (post-shock)	CEV (free-stream)
Height, km	-	81
Velocity, m/sec	391.8	7600.0
Temperature, K	6688.2	189.0
Number Density, $1/m^{-3}$	$1.98 \times 10^{+23}$	$2.9 \times 10^{+19}$
N Mole fraction	26.4%	0.0 %
O Mole Fraction	29.7%	1.595%
C Mole fraction	0.0%	0.0%
N_2 Mole Fraction	43.1%	78.685%
O_2 Mole Fraction	1.46×10^{-2} %	19.719%
NO Mole fraction	0.7%	0.0%
CO Mole fraction	0.0%	0.0%
CN Mole fraction	0.0%	0.0%

**TABLE 4.** Numerical parameters of the BGK and DSMC schemes

	BGK, 0 sec arcjet case	DSMC, 81 km CEV case
Number of cells	164,860	2,124,130
Number of particles	33,821,840	20,900,300
Timestep, sec	1.0×10^{-8}	1.0×10^{-8}
Number of processors	16	32
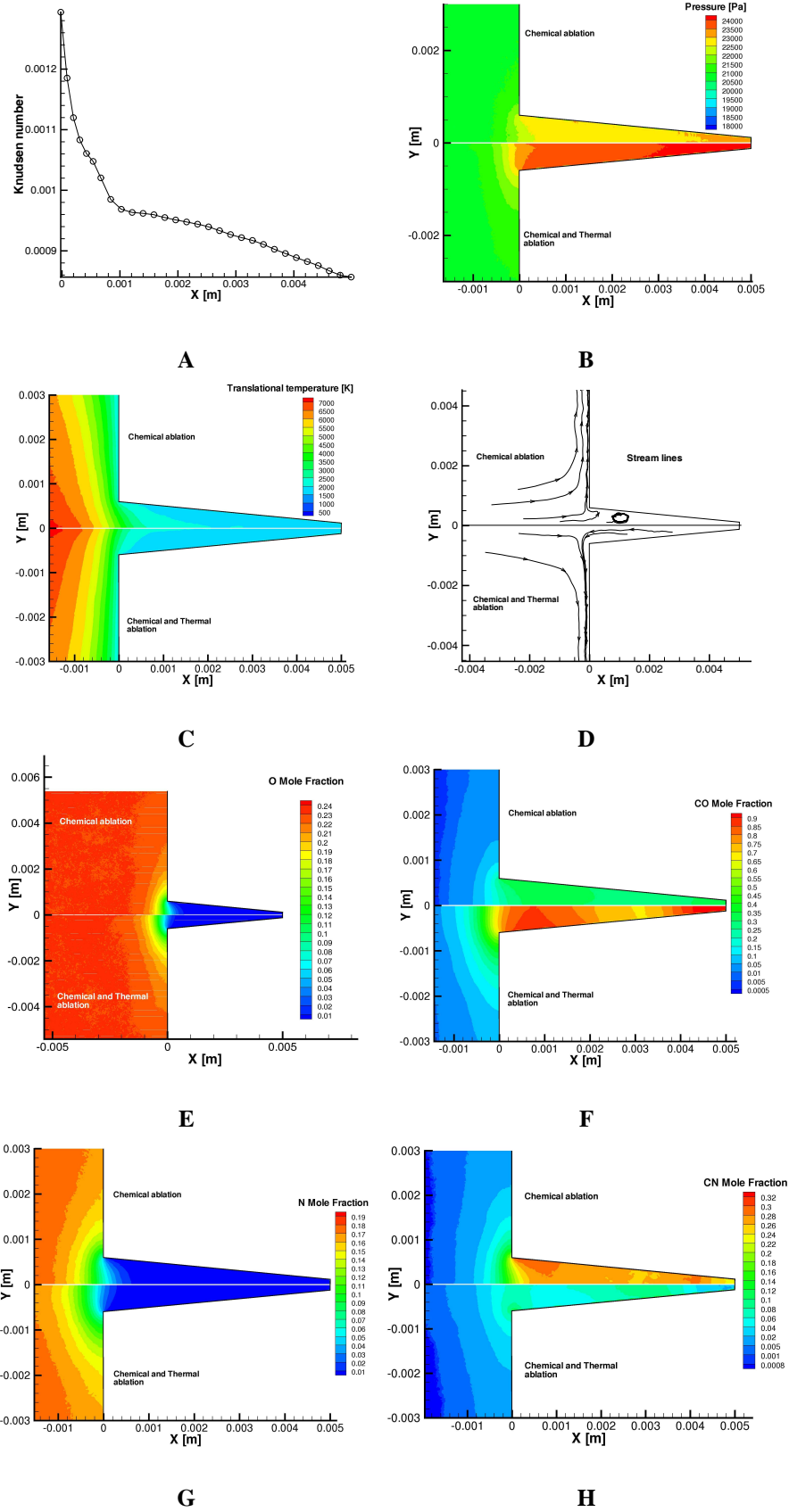
FIGURE 1. Arcjet 0 sec. BGK cases. A: Crack Knudsen number. Comparison of the major flow parameters for cases with chemical and with chemical an thermal ablation. B: pressure, C: translational temperature, D: stream lines. E: O mole fraction, F: CO mole fraction, G: N mole fraction, H: CN mole fraction.
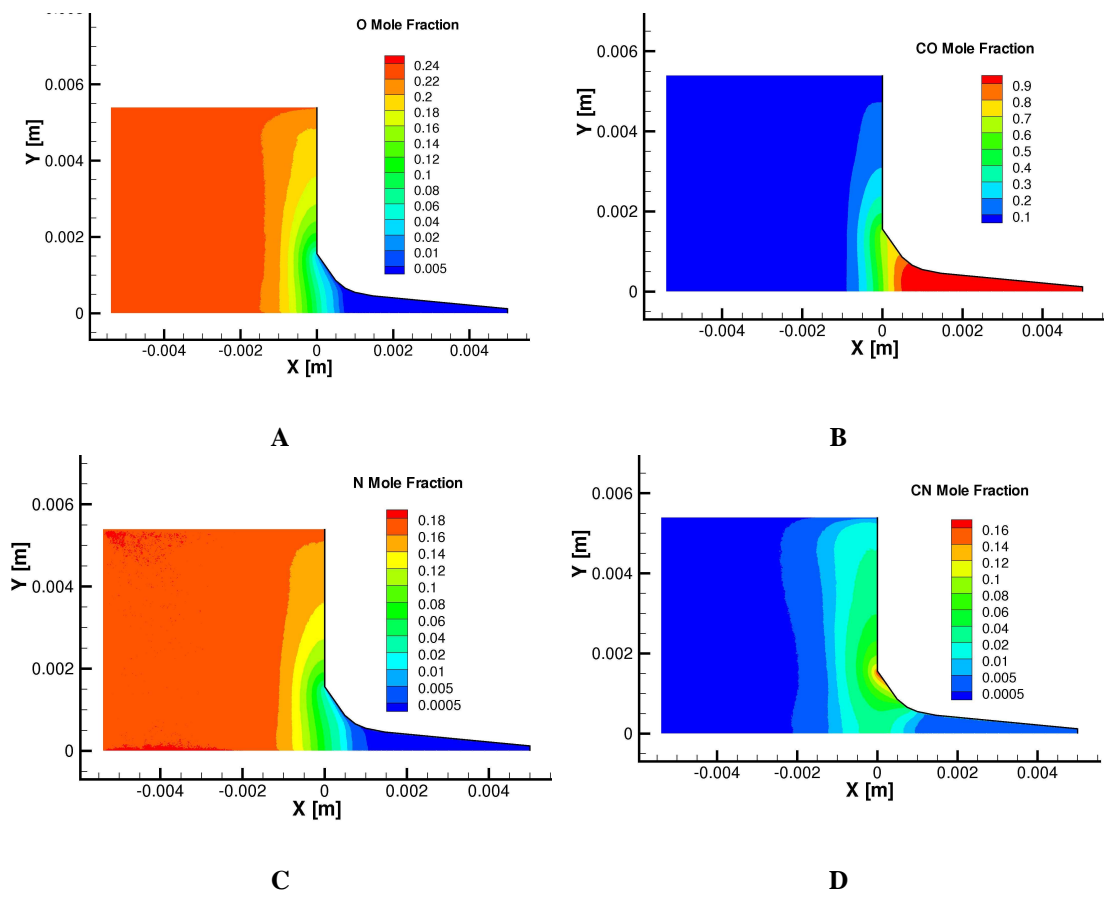
FIGURE 2. Arcjet 20 sec BGK case. Flow composition. A: O mole fraction, B: CO mole fraction, C: N mole fraction, D: CN mole fraction.
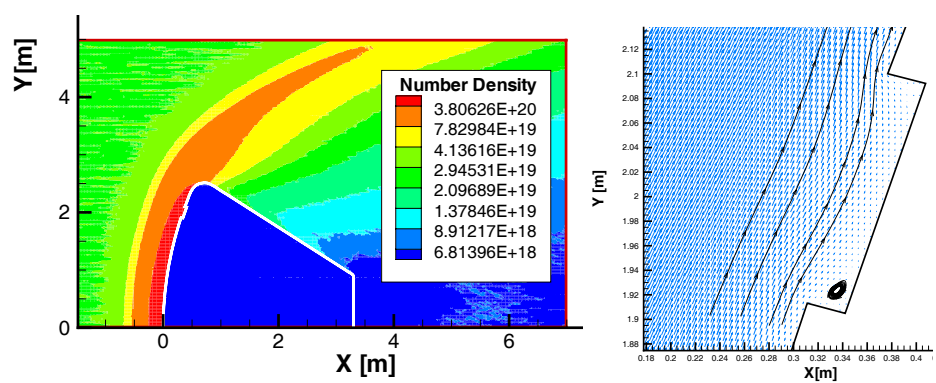
FIGURE 3. Compression pad case solution. DSMC simulations at 95 km.